

- vegetated areas or by 1 part atmospheric CO_2 ($\delta^{13}\text{C} = -7$ per mil) in arid regions with little or no vegetal covering [T. E. Cerling, *Earth Planet. Sci. Lett.* 71, 229 (1984)]. Amundson *et al.* [R. G. Amundson, O. A. Chadwick, J. M. Sowers, H. E. Doner, *Quat. Res.* 29, 245 (1988)] and Quade *et al.* (21) independently demonstrated that $\delta^{13}\text{C}$ of modern soil CO_2 in alluvial fans bordering the Spring Mountains decreases with increasing altitude (from 840 to 2740 m) and concomitant increasing plant density. Thus, the $\delta^{13}\text{C}$ of DIC can range from -13 to -4 per mil between regions of dense and no vegetation, respectively.
32. J. L. Betancourt, T. R. Van Devender, P. S. Martin, Eds., *Packrat Middens: The Last 40,000 Years of Biotic Change* (Univ. of Arizona Press, Tucson, 1990).
 33. W. G. Spaulding, in (32), pp. 166–199.
 34. _____, *U.S. Geol. Surv. Prof. Pap.* 1329 (1985).
 35. R. S. Thompson, in (32), pp. 200–239.
 36. A. Berger and P. Pestiaux, in *Milankovitch and Climate*, A. Berger, J. Imbrie, J. Hays, G. Kukla, B. Saltzman, Eds. (Reidel, Boston, 1984), part 1, pp. 83–111; A. L. Berger, *Quat. Res.* 9, 139 (1978).
 37. K. A. Maasch and R. J. Oglesby, *Paleoceanography* 5, 977 (1990).
 38. S. Manabe and A. J. Broccoli, *J. Geophys. Res.* 90, 2167 (1985).
 39. J. E. Kutzbach and P. J. Guetter, *J. Atmos. Sci.* 43, 1726 (1986).
 40. J. L. Bischoff, R. J. Rosenbauer, G. I. Smith, *Science* 227, 1222 (1985).
 41. I. C. Prentice, J. Guiot, S. P. Harrison, *Nature* 360, 658 (1992).
 42. G. Hut, Consultants' Group Meeting on Stable Isotope Reference Samples for Geochemical and Hydrological Investigations, Vienna, 16 to 18 September 1985. Report to Director General, International Atomic Energy Agency, Vienna, 42 (1987).
 43. We thank J. K. Böhlke, J. Thomas, E. Spiker, E. Sundquist, and T. E. Cerling for review comments; L. N. Plummer and F. J. Pearson Jr. for helpful discussions; and S. Andersen, J. Chen, J. Forsythe, C. Gwinn, and J. Hopple for excellent analytical aid.

2 August 1993; accepted 18 November 1993

Distinguishing the Direct and Indirect Products of a Gas-Surface Reaction

Charles T. Rettner and Daniel J. Auerbach

It has long been postulated that gas-surface chemical reactions can occur by means of two distinct mechanisms: direct reaction on a single gas-surface encounter or reaction between two adsorbed species. It is shown here that these mechanisms have distinct dynamical signatures, as illustrated by the reaction of hydrogen with chlorine on gold(111). The direct reaction product leaves the surface with a high kinetic energy in a narrow angular distribution that displays a "memory" of the direction and energy of the incident hydrogen atom. The indirect reaction product has a near-thermal energy distribution and an angular distribution that is close to that of a cosine function.

Gas-surface reactions are generally classified in terms of two idealized mechanisms (1). Some reactions are believed to occur more or less directly as a gas-phase reagent strikes an adsorbate, whereas other reactions are believed to involve reagents that are chemisorbed and in thermal equilibrium with the surface. We show that these two mechanisms can be distinguished by measuring the dynamical properties of the product. We illustrate this approach with results for the reaction of H with Cl on Au(111). We find that the direct reaction product leaves the surface with a high kinetic energy in a narrow angular distribution that displays a "memory" of the direction and energy of the incident H atom. In contrast, we find that the indirect reaction product has a near-thermal energy distribution and an angular distribution that is close to that of a cosine function.

The above-mentioned reaction mechanisms were proposed more than 70 years ago. Researchers at that time speculated that an impinging atom or molecule can

react directly upon striking an adsorbed species in a process that is now referred to as an Eley-Rideal (ER) mechanism. These researchers believed that reactions can also occur between species that have become fully accommodated to the surface in a process that is now referred to as a Langmuir-Hinshelwood (LH) mechanism. Although these mechanisms are consistent with chemical intuition and with observations of reaction rates (1–4), there was no direct evidence to support them. Such proof has been slow in coming. In 1922, Irving Langmuir (2) stated that, "With our increasing knowledge of the structure of solid bodies and of the atoms and molecules of which they are built we should now . . . gradually begin to gain a clear insight into the mechanisms of surface reactions." But only recently have we begun to gain the expected insight into mechanisms of surface reactions. The reason is simple. In order to probe reaction mechanisms [and to make contact with detailed calculations (5, 6)], one must go beyond structural and kinetic measurements to measurements of the nascent distributions of reaction products with re-

spect to angle (7), kinetic energy (7, 8), or internal state (9–11).

We have carried out such measurements for the reaction of H atoms with Cl adsorbed on a Au(111) surface. We show that the HCl product of this process is produced by both ER and LH mechanisms. Specifically, we have obtained information on the velocity and angular distributions of the HCl product. These measurements exhibit a clear bimodality that reflects the two mechanisms. Moreover, the HCl produced by the ER process has an angular distribution and a mean kinetic energy that depends on the kinetic energy of the incident H atom. Our results are consistent with a previous study of this system by Lykke and Kay (11). These researchers used laser ionization detection to determine the internal state distributions of the HCl product as a function of surface temperature. On the basis of their findings, Lykke and Kay were the first to suggest that this reaction might proceed by both ER and LH mechanisms. They were not, however, able to demonstrate correlations between initial state and final state properties, which are needed to prove that an ER mechanism applies.

The apparatus and techniques needed are similar to those used previously in studies of dissociation and inelastic scattering dynamics (7, 12). Beams of H atoms are chopped to produce short pulses and then directed at a Au(111) surface covered with a saturation layer of Cl (13). Two H atom beam sources are used. In one, the H_2 is dissociated by a microwave discharge in a quartz tube (14). This source gives H atoms with a mean kinetic energy of ~ 0.07 eV. The other source is based on thermal dissociation of H_2 in a graphite tube held at 2200 K (15). This source gives H atoms with a mean kinetic energy of ~ 0.3 eV. The angle of incidence of the H atoms is 60° from the surface normal in both cases. The Cl is supplied to the surface from a second beam

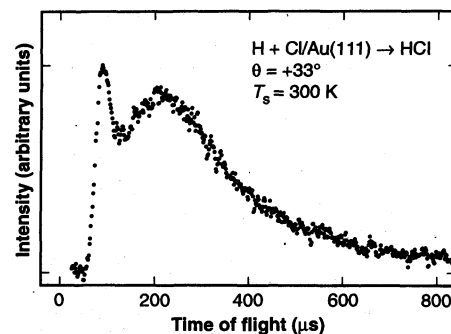


Fig. 1. Time-of-flight distribution of HCl formed by the reaction of H atoms with Cl/Au(111). This distribution was obtained for $T_s = 300$ K at a detection angle of 33° from the surface normal. The incident H atoms have a mean kinetic energy of 0.07 eV and an incidence angle of 60° .

IBM Research Division, Almaden Research Center, 650 Harry Road, San Jose, CA 95120.

source. The HCl reaction product is detected by a mass spectrometer that can be rotated about an axis passing through the crystal face to record products that leave the surface in specific directions. This instrument is also used to characterize the H beam directly.

Figure 1 displays the HCl signal recorded as a function of time after the opening of the chopper for a surface temperature, T_s , of 300 K. This time-of-flight (TOF) distribution is clearly bimodal. The relative intensities of the two peaks vary with detection angle, θ , and at 300 K the heights are approximately equal at $\theta = 33^\circ$. Figure 2 shows further results, recorded at $T_s = 300$ K for different values of θ . The variation of the intensities of the two components with θ is evident. The curves added to Fig. 2 correspond to fits that describe the distribution as the sum of two components from products with different velocity distributions. This analysis is similar to that described for inelastic scattering studies (16), but in this case the product velocity is assumed to be independent of the velocity of the incident atom. We find that the slow

components approximately follow a Maxwell-Boltzmann distribution of velocities, v , of the form

$$f(v) \propto v^3 \exp(-mv^2/2kT_{\text{eff}}) \quad (1)$$

where m is the mass, T_{eff} is an effective translational temperature, which is found to be close to T_s , and k is the Boltzmann constant. In contrast, the fast components require a form corresponding to a supersonic velocity distribution. We use

$$f(v) \propto v^3 \exp[-(v - v_0)^2/\alpha^2] \quad (2)$$

where v_0 is a stream velocity and α is a measure of the width of the distribution. No allowance is made for any residence time before the reaction. We find that the translational energy of the fast component is always relatively high. The values of v_0 and α are usually found to be in the range of 700 to 1000 m s^{-1} , yielding mean energies of ~ 0.6 eV with a high energy tail that extends up to about 2 eV, which is the full exothermicity of the reaction for an ER mechanism. Because the LH mechanism is believed to be almost thermoneutral, this high energy strongly suggests that the fast component arises from an ER mechanism. The velocity distributions of the late (slow) components are, however, consistent with an LH mechanism, one in which the product is accommodated before desorption. The difference between the energy distributions that we obtain for the two different components can be seen in Fig. 3. It displays the approximate energy distributions for the slow (LH) and fast (ER) components, deduced from fits to TOF distributions obtained at $T_s = 300$ K and $\theta = 0^\circ$ with the incidence energy (E_i) = 0.07 eV. The assignment of the slow component to an LH mechanism is further supported by the fact that this contribution to the TOF distributions disappears for $T_s < 170$ K. This point is illustrated in Fig. 4, which

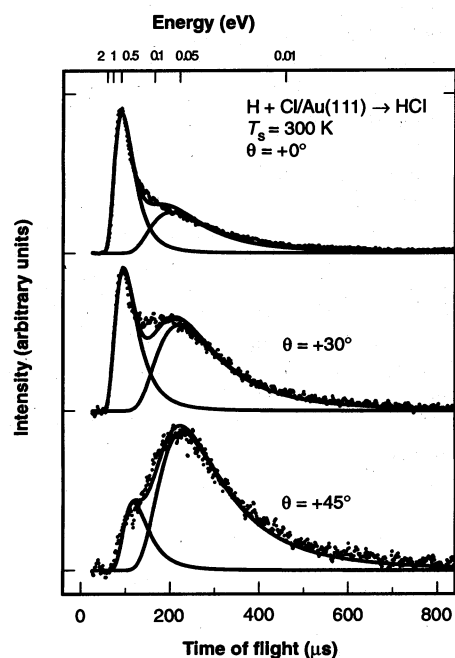


Fig. 2. Time-of-flight distributions of HCl formed by the reaction of H atoms with Cl/Au(111) for $T_s = 300$ K for detection angles of 0° , 30° , and 45° with respect to the surface normal. The incident H atoms have a mean kinetic energy of 0.07 eV and an incidence angle of 60° . The curves indicate the results of fits to the data. The energy axis along the top of the figure is only approximate. Accurate energies are obtained by the fitting procedure described in the text, which yields mean kinetic energies for the fast components of ~ 0.6 , 0.5, and 0.25 eV, for $\theta = 0^\circ$, 30° , and 45° , respectively. In each case, the slower components follow Boltzmann distributions close to T_s (that is, $T_{\text{eff}} \sim T_s$).

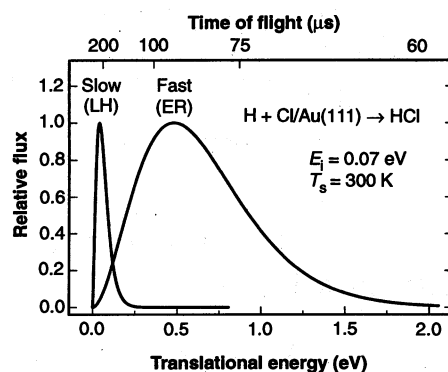


Fig. 3. Translational energy distributions of the HCl product of the reaction of H atoms with Cl/Au(111) for the Eley-Rideal (ER) and Langmuir-Hinshelwood (LH) mechanisms. These distributions were obtained from fits to the TOF distributions as displayed in Fig. 2. These particular distributions correspond to $T_s = 300$ K and $\theta = 0^\circ$. The TOF axis indicates the approximate corresponding flight times.

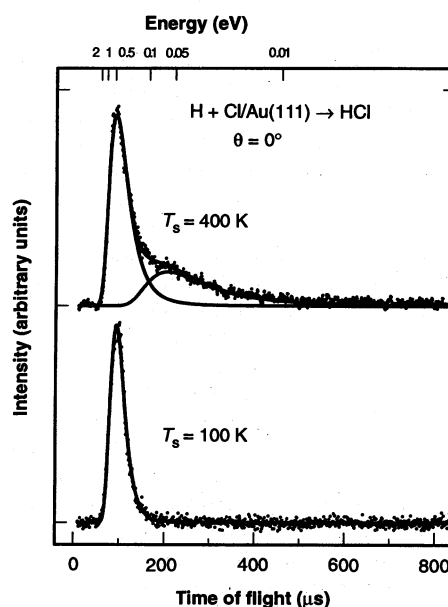


Fig. 4. Time-of-flight distributions of HCl formed by the reaction of H atoms with Cl/Au(111) for $T_s = 400$ and 100 K for $\theta = 0^\circ$. The incident H atoms have a mean kinetic energy of 0.07 eV and an incidence angle of 60° . The energy axis is only approximate. The curves indicate the results of fits to the data. The mean kinetic energy of the fast components is ~ 0.6 eV.

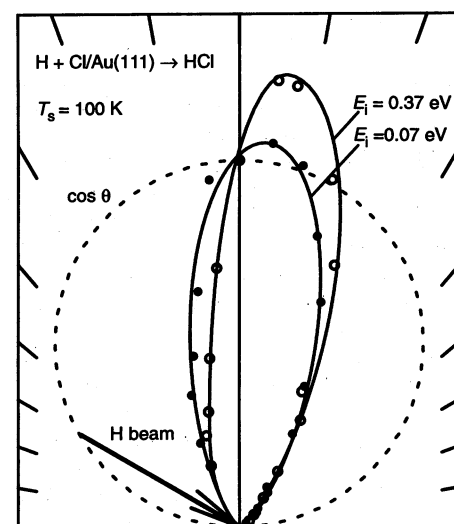


Fig. 5. Polar plot of the angular distributions of the HCl product of the reaction of H atoms with Cl/Au(111) for $T_s = 100$ K. (Signal intensities are proportional to the distance from the origin.) Results are displayed for incidence energies of 0.07 and 0.37 eV, as labeled. The angle of the incidence beam (60°) is indicated graphically by the arrow. These results are attributed to an ER mechanism. The broken line corresponds to $\cos \theta$, which is expected in the absence of dynamical factors. The ticks are placed at 10° intervals.

shows a comparison of results for $\theta = 0^\circ$, with $T_s = 400$ and 100 K. These observations suggest that for the higher surface temperature, the HCl product is formed through two distinct reaction mechanisms, one of which is "frozen out" at the lower surface temperature.

We obtained further dynamical evidence for these two assumed mechanisms by changing the energy of the incident H beam and from the form of the angular distributions. For $\theta = 0^\circ$, changing the mean energy of the incident H atoms from 0.07 to 0.3 eV results in an increase in the mean translational energy of the HCl product from ~ 0.50 to ~ 0.56 eV. Such behavior clearly indicates an essentially direct reaction process. The angular distributions support this model. The angular distributions of the fast component for H atom beams with mean energies of 0.07 and 0.3 eV are shown in Fig. 5. The fact that these distributions are asymmetric with respect to the surface normal and that they change with the incidence energy implies that the HCl product retains a memory of the momentum of the incident H atom. Such a result is inconsistent with an LH mechanism but rather shows that the reaction occurs directly, by way of an ER mechanism. We obtained further information by analyzing TOF distributions obtained at different values of θ for the 0.3 -eV beam. We find that the mean energy of the HCl product associated with the fast component rises to ~ 0.8 eV for values of θ of $\sim 20^\circ$ on either side of the normal. This behavior indicates that there is a strong correlation between the exit angle and the energy released in translation. A study of such effects as a function of incidence energy might elucidate this behavior.

In contrast to the fast component, the angular distribution of the slow component is found to be symmetric with respect to the surface normal, following a distribution that is slightly narrower than a cosine. The actual distribution is well described by a cosine function raised to the power of 1.4 . The slight narrowing with respect to a true cosine is somewhat surprising. One possibility is that this component contains a small contribution from an ER-type mechanism that involves multiple "bounces" (17). Ideally, such questions could be better addressed by measuring angle and velocity distributions for products in specific quantum states.

Many questions remain for this system: Does the ER channel involve a single collision or can the H atom "bounce" before reacting? Why do some collisions lead to ER and others to LH mechanisms? What determines the branching ratio? Our results, together with other recent studies (7–11), set a firm foundation for such ques-

tions. We believe that such dynamical studies are a prerequisite to understanding surface chemistry in terms of atomic and molecular motions.

REFERENCES

1. See, for example, W. H. Weinberg, in *Dynamics of Gas-Surface Interactions*, C. T. Rettner and M. N. R. Ashfold, Eds. (Royal Society of Chemistry, London, 1991), pp. 171–219.
2. I. Langmuir, *Trans. Faraday Soc.* **17**, 621 (1922).
3. C. C. Cheng, S. R. Lucas, H. Gutleben, W. J. Choyke, Y. T. Yates, *J. Am. Chem. Soc.* **114**, 1249 (1992).
4. M. Xi and B. E. Bent, *J. Vac. Sci. Technol. B* **10**, 2440 (1992).
5. P. Kratzer and W. Brenig, *Surf. Sci.* **254**, 275 (1991).
6. B. Jackson and M. Persson, *J. Chem. Phys.* **96**, 2378 (1992).
7. C. T. Rettner, *Phys. Rev. Lett.* **69**, 383 (1992).
8. E. W. Kuipers, A. Vardi, A. Danon, A. Amirav, *ibid.* **66**, 116 (1991).
9. R. I. Hall, I. Cadez, M. Landau, F. Pichou, C. Schermann, *ibid.* **60**, 337 (1988).
10. P. J. Eenshuistra, J. H. M. Bonnie, J. Loss, H. J. Hopmann, *ibid.*, p. 341.
11. K. Lykke and B. D. Kay, in *SPIE Proc.* **1208**, 18 (1990).
12. C. T. Rettner, L. A. DeLouise, D. J. Auerbach, *J. Chem. Phys.* **85**, 1131 (1986).
13. G. N. Kastanas and B. E. Koel, *Appl. Surf. Sci.* **64**, 235 (1993).
14. C. T. Rettner, H. A. Michelsen, D. J. Auerbach, C. B. Mullins, *J. Chem. Phys.* **94**, 7499 (1991).
15. D. J. Auerbach and C. T. Rettner, *Rev. Sci. Instrum.* **63**, 3939 (1992).
16. C. T. Rettner, E. K. Schweizer, C. B. Mullins, *J. Chem. Phys.* **90**, 3800 (1989).
17. J. Harris and B. Kasemo, *Surf. Sci.* **105**, L281 (1981).

27 September 1993; accepted 17 November 1993

High-Performance Photorefractive Polymers

Martin Liphardt, Arosha Goonesekera, Brian E. Jones, Stephen Ducharme,* James M. Takacs, Lei Zhang

Photorefractive materials can form "instant" holograms without time-consuming development steps. Their potential applications include image processing, optical data storage, and correction of image distortion, but the cost of crystal growth and preparation has been a primary impediment to commercial application. Polymers, on the other hand, are low in cost and readily fabricated in a variety of forms. Photorefractive polymers were constructed with performance that matched or exceeded the performance of available photorefractive crystals. The largest observed two-beam energy coupling gain coefficient for the polymers was 56 per centimeter.

The photorefractive effect, a persistent but reversible change in the refractive index of an electrooptic material caused by nonuniform illumination, was first observed as a detrimental "optical damage" in lithium niobate and other crystals used for second harmonic generation (1). The photorefractive effect occurs in materials that have the following three properties: (i) photoconduction, (ii) photosensitive traps, and (iii) linear electrooptic response. Nonuniform illumination liberates charges from the photosensitive traps in the bright regions. These charges diffuse and drift until they recombine with ionized traps elsewhere. After some time, charge is depleted from the bright regions and added to the dark regions, creating a spatially varying, or space-charge, electric field. The space-charge electric field changes the index of refraction through the linear electrooptic (Pockels) effect, creating a replica, or phase hologram, of the original

intensity pattern. This hologram persists in the dark. Photorefractive materials can be used in image processing applications such as image correlation (2), amplification (3), and dynamic novelty filtering (4). Data can be stored in photorefractive materials in the form of the three-dimensional phase holograms, which have very high density and can be accessed by fast parallel optical retrieval (5) or associative retrieval with incomplete addressing (6). Photorefractive materials have been used to correct phase distortions suffered by an optical beam in inhomogeneous (7) or turbulent media (8). These and many other applications have been demonstrated with high-performance photorefractive crystals.

Polymers that exhibit the photorefractive effect have been made (9–12). These hybrid materials combine electrooptic polymers with charge transport agents and photosensitizing dyes. Photorefractive polymers may replace crystals in future applications because of their relative low cost. Polymers are also amenable to mass production in a variety of forms satisfying complex requirements imposed by device performance and operating environment; polymers can be cast, spun, painted, molded, injected, or extrud-

M. Liphardt, A. Goonesekera, B. E. Jones, S. Ducharme, Department of Physics and Astronomy, University of Nebraska, Lincoln, NE 68588-0111. J. M. Takacs and L. Zhang, Department of Chemistry, Center for Materials Research and Analysis, University of Nebraska, Lincoln, NE 68588-0304.

*To whom correspondence should be addressed.